Journal of Molecular Spectroscopy 316 (2015) 54–63

Contents lists available at ScienceDirect

Journal of Molecular Spectroscopy

journal homepage: www.elsevier.com/locate/jms

High-resolution infrared spectrum of triacetylene: The ν_5 state revisited and new vibrational states

K.D. Doney *, D. Zhao, H. Linnartz

Sackler Laboratory for Astrophysics, Leiden Observatory, University of Leiden, PO Box 9513, NL 2300 RA Leiden, The Netherlands

ARTICLE INFO

Article history:
Received 5 June 2015
In revised form 24 July 2015
Available online 29 July 2015

Keywords:
Infrared spectroscopy
Triacetylene
Vibrationally excited
cw-CRDS
Supersonic plasma jet

ABSTRACT

New data are presented that follow from a high-resolution survey, from 3302 to 3352 cm^{-1}, through expanding acetylene plasma, and covering the C—H asymmetric (ν_5) fundamental band of triacetylene (HC_6H). Absorption signals are recorded using continuous wave cavity ring-down spectroscopy (cw-CRDS). A detailed analysis of the resulting spectra allows revisiting the molecular parameters of the ν_5 fundamental band in terms of interactions with a perturbing state, which is observed for the first time. Moreover, four fully resolved hot bands ($5_0^1 10_1^1$, $5_0^1 11_1^1$, $5_0^1 13_1^1$, and $1_0^1 8_0^1 11_1^0$), with band origins at 3328.5829(2), 3328.9994(2), 3328.2137(2) and 3310.8104(2) cm^{-1}, respectively, are reported for the first time. These involve low lying bending vibrations that have been studied previously, which guarantees unambiguous identifications. Combining available data allows to derive accurate molecular parameters, both for the ground state as well as the excited states involved in the bands.

1. Introduction

Polyynes (*i.e.* polyacetylenes; of the generic form $HC_{2n}H$) are believed to play an important role in combustion chemistry, and in a variety of different astrochemical environments [1–8]. The linear, unsaturated structure of polyynes results in a class of molecules which are unstable and highly reactive. Through barrier-less, polymerization reactions, *e.g.*

$$H{-}C{\equiv}C{-}C{\equiv}C{-}H + {\bullet}C{\equiv}C{-}H \rightarrow H{-}C{\equiv}C{-}C{\equiv}C{-}C{\equiv}C{-}H + H \quad (1)$$

small polyynes can act as intermediates to the formation of larger molecules, such as longer chain (cyano) polyynes, polycyclic aromatic hydrocarbons, and "soot" [1,9–14].

Of notable interest is triacetylene (HC_6H), which has only been observed in the protoplanetary nebulae, CRL 618 and SMP LMC 11 through the $\nu_8 + \nu_{11}$ and ν_{11} bands [3,6], but not in the prototypical carbon rich environments of Titan, TMC-1, or the AGB star IRC + 10 216, where both acetylene and diacetylene, polyyne radicals (C_nH) up to $n = 8$, and the anionic radical C_6H^-, have been observed [15–17]. Also, the cumulene isomer of H_2C_6, which is less stable compared to triacetylene [18], has been detected in TMC-1 [19]. Given that the acetylenic isomer is energetically favored over the cumulene isomer, the low probability of isomerization between the two forms, and observation of the radical form of triacetylene (C_6H) [20,21], it is expected that triacetylene will be present in other carbon rich environments as well.

One of the particular reasons for the missing detections of polyynes compared to their respective radical or cyano-form is that the polyyne molecules are difficult to observe in the infrared at the typical temperatures found in most astronomical objects, and the lack of a permanent dipole moment associated with centro-symmetric molecules means that for polyynes pure rotational transitions are forbidden, excluding radio astronomical detections. Certain vibrational modes will induce a temporary dipole moment that can be detected as ro-vibrational spectra in the mid- and far-infrared. While, the spectroscopic information of both acetylene and diacetylene has been studied in detail in laboratory studies facilitating their detection (see Zhao et al. [22] and Chang and Nesbitt [23] and references therein), the spectroscopic information for triacetylene so far has remained limited. Vibrational frequencies for the fundamental bands of triacetylene, Table 1, have been known with a resolution of 1 cm^{-1} [24], but high-resolution rotational information is only known for about half of the modes: ν_5, ν_6, ν_8, ν_{10}, ν_{11}, and ν_{13} [25–28]; it is noted that ν_8 and ν_{10} rotational information is determined from the $8_0^1 11_0^1$ combination band and the $8_0^1 11_0^1 10_1^1$ and $11_0^1 10_1^1$ hot bands, respectively [25]. We adopt here conventional vibronic notation to indicate lower/upper states of each vibrational mode in a transition. Past experiments by Matsumura et al. [26] noted that the C—H stretch fundamental band is highly perturbed at $J' = 20$ and 50 and 54, and predicted three major hot bands $5_0^1 13_1^1$, $5_0^1 13_2^2$, and $5_0^1 10_1^1$ to be 60%, 35%,

* Corresponding author.
E-mail address: doney@strw.leidenuniv.nl (K.D. Doney).

http://dx.doi.org/10.1016/j.jms.2015.07.007
0022-2852/

Table 1
Vibrational normal modes of triacetylene (cm^{-1}).

	State	Motion	Obs. freq.
ν_1	Σ_g^+	C—H sym. stretch	3313(1)[a]
ν_2		terminal C≡C sym. stretch	2201(1)[a]
ν_3		internal C≡C sym. stretch	2019(1)[a]
ν_4		internal C—C sym. stretch	625(1)[a]
ν_5	Σ_u^+	C—H asym. stretch	3329.0533(1)[b]
ν_6		terminal C≡C asym. stretch	2128.91637(32)[c]
ν_7		internal C≡C asym. stretch	1115.0(5)[d]
ν_8	Π_g	C≡C—H sym. bend	622.38(40)[e]
ν_9		terminal C≡C—C sym. bend	491(1)[a]
ν_{10}		internal C≡C—C sym. bend	258(1)[a]
ν_{11}	Π_u	C≡C—H asym. bend	621.340111(42)[f]
ν_{12}		terminal C≡C—C asym. bend	443.5(5)[d]
ν_{13}		internal C≡C—C asym. bend	105.038616(76)[d]

[a] Ref. [24].
[b] This work.
[c] Ref. [25].
[d] Ref. [27].
[e] Ref. [29].
[f] Ref. [28].

and 28% the intensity of the ν_5 fundamental at room temperature [26].

In this work we present an extended high-resolution infrared study of the ro-vibrational transitions of triacetylene in the C—H stretch fundamental region. We have observed the ν_5 fundamental band of triacetylene and transitions to one of its perturbing levels, three hot bands associated with the ν_5 mode that are due to doubly degenerate bending vibrational modes (ν_{10}, ν_{11}, and ν_{13}), and one hot bands associated with the ν_1 mode, for which a complete analysis is given here.

2. Experimental details

The experimental setup combines pulsed supersonic planar plasma with continuous wave cavity ring-down spectroscopy (cw-CRDS), and has been described in detail by Zhao et al. [30], following Motylewski and Linnartz [31]. Given recent experiments by our group on diacetylene [22], which also produced triacetylene but in lower concentrations, we have been investigating different sets of experimental settings to discriminate weaker signals. It is found that the optimal conditions to produce triacetylene are by discharging a gas mixture of 0.3% C_2H_2 diluted in Ar with an applied negative high voltage of ~−525 V. Each gas pulse (~1 ms) has a typical backing pressure of ~15 bar, and is supersonically expanded through a 30 mm × 0.3 mm multi-layer slit discharge nozzle mounted to a pulsed valve (General Valve, Series 9, 2 mm orifice) into a vacuum chamber, which is kept at a few 10^{-2} mbar by a roots blower pump station (4800 m^3/h). The discharge nozzle is aligned with the slit throat parallel to and ~3 cm, away from the optical axis of a high finesse optical cavity. The optical cavity is formed by two highly reflective plano-concave mirrors (1 m radius of curvature, reflectivity ~99.97% at 3 μm) mounted on precision alignment tools 56 cm apart on opposite sides of the main chamber. In order to insure the mirrors retain their high reflectivity throughout the plasma discharge, N_2 is flowed in front of the reflective surface of each mirror.

The high-resolution infrared spectrum of the plasma products is recorded using cw-CRDS. The idler output of a commercial single-frequency single-mode continuous wave optical parametric oscillator (cw-OPO, Aculight, Argos 2400-SF module B), operating between ~3000 and 4000 cm^{-1} with an output power of ⩽1.2 W and a bandwidth of <1 MHz, is employed as the infrared light source. The infrared beam is subsequently split in order to simultaneously measure the laser frequency and perform ring-down measurements. A fraction of the light is directed to a wavelength meter (Bristol Instruments, 621A-IR, self-calibrated by a stabilized He–Ne laser), which provides relative and absolute frequency accuracies better than 6 MHz and 20 MHz, respectively. Simultaneously, the remainder of the idler is led through an acousto-optical modulator (AOM), and the first order deflection, ~5% of the power, is coupled into the optical cavity. Given that the idler wavelength is continuously changed during a scan, a piezo-electric transducer with a periodic triangle applied voltage is mounted on one of the mirror holders, behind the mirror, to

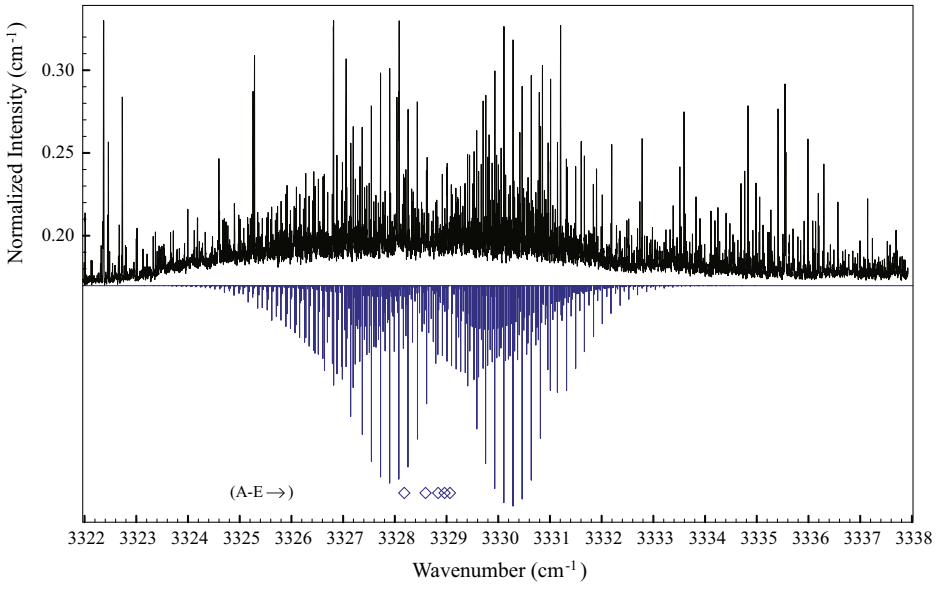

Fig. 1. A portion of the spectrum highlighting the observed bands related to the C—H asymmetric stretch; the experimental spectrum is plotted on top in black, and the simulated spectrum of the identified triacetylene bands is plotted below in blue. The band origins are marked with empty diamonds in increasing frequency order: (A) $5_0^1 13_1^1$, (B) $5_0^1 10_1^1$, (C) the perturber state of 5_0^1, (D) $5_0^1 11_1^1$, and (E) 5_0^1. The remaining absorption features are due to other molecules in the plasma, most of which are assigned to acetylene and diacetylene [22]. (For interpretation of the references to colour in this figure legend, the reader is referred to the web version of this article.)

Table 2
Lower and upper state rotational and centrifugal distortion constants for the ν_5 fundamental band and perturber band of triacetylene (cm^{-1}).[a]

		Coriolis interaction[b]		Fermi resonance[b]		Matsumura et al. [26]	
	Ground	ν_5	Perturber	ν_5	Perturber	Ground	ν_5
Symmetry	Σ_g^+	Σ_u^+	Π_u	Σ_u^+	Σ_u^+	Σ_g^+	Σ_u^+
Band origin		3329.0544(1)	3328.8584(2)	3329.0521(1)	3328.8435(2)		3329.05164(49)
B	0.0441735(12)	0.0441377(2)	0.0443102(14)	0.0441377(2)	0.0445931(32)	0.04417088(75)	0.04413523(87)
$q \times 10^4$			4.766(7)				
$D \times 10^8$	0.107(7)	0.137(6)	0.308(293)	0.137(7)	1.66(63)	0.0930(43)	0.1245(131)
$H \times 10^{12}$		0.020(7)		0.020(7)			0.0207(132)
$L \times 10^{18}$		−0.523(233)		−0.505(252)			−0.558(477)
		$\zeta = 6.86(5) \times 10^{-4}$		$W = 2.18(2) \times 10^{-2}$			

[a] Uncertainty corresponding to one standard deviation given in the parentheses.
[b] Simultaneous analysis of jet-cooled data and high-J data from Matsumura et al. [26] to determine constants.

Table 3
Lower and upper state rotational and centrifugal distortion constants for the hot bands of triacetylene (cm^{-1}).[a]

Level	Symmetry	Band origin	B''	$q'' \times 10^5$	$D'' \times 10^8$	B'	$q' \times 10^5$	$D' \times 10^8$
$1_0^1 8_0^1 11_1^{0}$[b]	$\Pi_g - \Pi_u$	3310.8104(2)	0.0441827	0.78	0.0973	0.0441528(9)	0.83(10)	
$5_0^1 10_1^1$	$\Pi_u - \Pi_g$	3328.5829(2)	0.0442534(7)	1.62(4)	0.16(8)	0.0442216(9)	1.60(4)	0.67(8)
$5_0^1 11_1^{1}$[b]	$\Pi_g - \Pi_u$	3328.9994(2)	0.0441827	0.78	0.0973	0.0441465(6)	0.73(9)	
$5_0^1 13_1^{1}$[c]	$\Pi_g - \Pi_u$	3328.2137(2)	0.0442588	3.82	0.09683	0.0442268(7)	3.72(3)	0.48(5)

[a] Uncertainty corresponding to a standard deviation given in the parentheses.
[b] Lower state constants are fixed to Haas et al. [28].
[c] Lower state constants are fixed to Haas et al. [27].

Table 4
Observed line positions in cm^{-1} assigned to the ν_5 fundamental band of triacetylene with coriolis interaction.

Transition	Obs.	$o-c \times 10^4$	Transition	Obs.	$o-c \times 10^4$	Transition	Obs.	$o-c \times 10^4$
P(37)	3325.7333	−8	P(8)	3328.3451	−8	R(18)	3330.7271	2
P(35)	3325.9156	−1	P(7)	3328.4345	−2	R(19)	3330.8186	11
P(33)	3326.0970	1	P(6)	3328.5228	−6	R(20)	3330.9118	9
P(31)	3326.2771	−6	P(5)	3328.6112	−9	R(21)	3330.9646	16
P(29)	3326.4618*	39	P(4)	3328.6990	−16	R(22)	3331.0559	17
P(27)	3326.6361	−10	P(3)	3328.7874	−18	R(23)	3331.1459	23
P(24)	3326.9030	9	P(2)	3328.8749	−27	R(24)	3331.2275*	−43
P(23)	3326.9873	−2	R(1)	3329.2291	−18	R(25)	3331.3180	−14
P(22)	3327.1116	−5	R(3)	3329.4074	2	R(26)	3331.4067	2
P(21)	3327.1955	1	R(5)	3329.5832	0	R(27)	3331.4971*	37
P(20)	3327.2813	−1	R(6)	3329.6711	−1	R(28)	3331.5766*	−35
P(19)	3327.3688	0	R(7)	3329.7595	5	R(29)	3331.6660	−5
P(18)	3327.4570	−1	R(8)	3329.8472	4	R(30)	3331.7526	−3
P(17)	3327.5460	2	R(9)	3329.9349	3	R(31)	3331.8392	0
P(16)	3327.6342	−3	R(10)	3330.0229	6	R(32)	3331.9254	1
P(15)	3327.7234	−1	R(11)	3330.1104	3	R(33)	3332.0116	3
P(14)	3327.8121	−4	R(12)	3330.1986	8	R(34)	3332.0973	1
P(13)	3327.9010	−4	R(13)	3330.2866	11	R(35)	3332.1831	1
P(12)	3327.9903	−1	R(14)	3330.3739	6	R(36)	3332.2681	−6
P(11)	3328.0796	2	R(15)	3330.4622	11	R(37)	3332.3533	−11
P(10)	3328.1680	−3	R(16)	3330.5506	14	R(38)	3332.4385	−15
P(9)	3328.2565	−6	R(17)	3330.6390	13			

Lines not included in the fit are indicated by *.

modulate the cavity length such that the cavity is in resonance with the infrared laser at least twice during one period. Only when the light is effectively coupled into the cavity does the light intensity trigger a hardware (Boxcar integrator) based multi-trigger timing scheme, which coincides a plasma pulse to one ring-down event and is described in detail in Zhao et al. [30]. Typical ring-down times are ~7 μs, corresponding to roughly 4000 effective passes of the infrared laser through the plasma jet. An absorption spectrum is recorded by measuring ring-down times as a function of infrared laser frequency. The absolute frequency calibration is determined to be ~0.001 cm^{-1} by checking the frequencies of the recorded absorption spectrum of the precursor gas, C_2H_2, against the corresponding HITRAN values [32].

3. Results and discussion

The high-resolution spectrum is recorded between 3302 and 3352 cm^{-1} (Fig. 1). Two particularly dense forests of lines are seen in the experimental spectrum centered at 3314 and 3330 cm^{-1}. Preliminary analysis based on previous work on HC_4H [22,33], and the vibrational frequencies of HC_6H (Table 1), hints for assignment of the first region around 3314 cm^{-1} to the C—H symmetric stretch mode region, and the region around 3330 cm^{-1} to the C—H asymmetric stretch mode region. The experimental spectrum shows features assigned to the C—H asymmetric stretch fundamental mode of acetylene and diacetylene, and a number of hot bands of diacetylene, which have been described in detail in

Table 5
Observed line positions in cm^{-1} assigned to the ν_5 fundamental band of triacetylene with fermi resonance.

Transition	Obs.	$o-c \times 10^4$	Transition	Obs.	$o-c \times 10^4$	Transition	Obs.	$o-c \times 10^4$
P(37)	3325.7333	−8	P(8)	3328.3451	−7	R(18)	3330.7271	1
P(35)	3325.9156	−1	P(7)	3328.4345	−1	R(19)	3330.8186	8
P(33)	3326.0970	1	P(6)	3328.5228	−5	R(20)	3330.9118	0
P(31)	3326.2771	−5	P(5)	3328.6112	−8	R(21)	3330.9646	16
P(29)	3326.4618*	39	P(4)	3328.6990	−16	R(22)	3331.0559	16
P(27)	3326.6361	−10	P(3)	3328.7874	−17	R(23)	3331.1459	23
P(24)	3326.9030	8	P(2)	3328.8749	−26	R(24)	3331.2275*	−44
P(23)	3326.9873	−2	R(1)	3329.2291	−17	R(25)	3331.3180	−14
P(22)	3327.1116	−14	R(3)	3329.4074	3	R(26)	3331.4067	2
P(21)	3327.1955	−2	R(5)	3329.5832	1	R(27)	3331.4971*	37
P(20)	3327.2813	−2	R(6)	3329.6711	0	R(28)	3331.5766*	−35
P(19)	3327.3688	0	R(7)	3329.7595	6	R(29)	3331.6660	−5
P(18)	3327.4570	−1	R(8)	3329.8472	5	R(30)	3331.7526	−3
P(17)	3327.5459	3	R(9)	3329.9349	4	R(31)	3331.8392	1
P(16)	3327.6342	−3	R(10)	3330.0229	6	R(32)	3331.9254	2
P(15)	3327.7234	0	R(11)	3330.1104	4	R(33)	3332.0116	3
P(14)	3327.8121	−3	R(12)	3330.1986	9	R(34)	3332.0973	1
P(13)	3327.9010	−3	R(13)	3330.2866	12	R(35)	3332.1831	1
P(12)	3327.9903	0	R(14)	3330.3739	7	R(36)	3332.2681	−6
P(11)	3328.0796	3	R(15)	3330.4622	12	R(37)	3332.3533	−11
P(10)	3328.1680	−2	R(16)	3330.5506	14	R(38)	3332.4385	−14
P(9)	3328.2565	−6	R(17)	3330.6390	13			

Lines not included in the fit are indicated by *.

Table 6
Observed line positions in cm^{-1} assigned to the perturber band of the ν_5 fundamental band of triacetylene with coriolis interaction.

Transition	Obs.	$o-c \times 10^4$
P(23)	3327.0320	−6
P(22)	3327.0681	−17
P(21)	3327.1483	−8
P(20)	3327.2253	−9
P(19)	3327.3017	−9
P(17)	3327.4565	11
R(19)	3330.7722	11
R(20)	3330.8695	8
R(21)	3331.0082	2
R(22)	3331.1076	−14
R(23)	3331.2172*	47
R(24)	3331.3180	2
R(25)	3331.4245	1
R(26)	3331.5321	1

Lines not included in the fit are indicated by *.

Table 7
Observed line positions in cm^{-1} assigned to the perturber band of the ν_5 fundamental band of triacetylene with fermi resonance.

Transition	Obs.	$o-c \times 10^4$
P(25)	3326.8889	7
P(24)	3326.9591	−9
P(23)	3327.0320	−25
P(22)	3327.0667	−27
P(21)	3327.1483	4
P(19)	3327.2990	0
R(17)	3330.5680	2
R(19)	3330.7722	23
R(20)	3330.8693	10
R(21)	3331.0083	−17
R(22)	3331.1125	3
R(23)	3331.2174	3

Zhao et al. [22]. Additionally, based on a rotational line spacing of ~0.044 cm^{-1}, six bands of triacetylene are identified in the experimental spectrum.

Effective band origins, and rotational and centrifugal distortion constants for the lower and upper states of each band are determined using PGOPHER software [34], starting from a standard ro-vibrational Hamiltonian for linear molecules:

$$H = H_{vib} + B\mathbf{N}^2 - D\mathbf{N}^4 + H\mathbf{N}^6 + L\mathbf{N}^8 \quad (2)$$

which gives the following expression of ro-vibrational energy levels (v, l, J)

$$E(v,l,J) = G_{v,l} + B_v[J(J+1) - l^2] - D_v[J(J+1) - l^2]^2 + H_v[J(J+1) - l^2]^3 + L_v[J(J+1) - l^2]^4 \quad (3)$$

where H_{vib} is the vibrational Hamiltonian, $\mathbf{N}$ is the rotational angular momentum ($\mathbf{N} = \mathrm{J} + \mathrm{L}$), $G_{v,l}$ the vibrational energy, B_v the rotational constant, and D_v, H_v and L_v are the quartic, sextic, and octic centrifugal distortion constants, respectively, of the corresponding vibrational level. For the degenerate vibrational levels, $l > 0$, where l is the quantum number related to the projection of the total vibrational angular momentum on the symmetry axis, the l-type doubling constant, q, is required, and is fit by the operator [34]

$$\frac{1}{2}\mathbf{N}_+^2 L_-^2 + \mathbf{N}_-^2 L_+^2 \quad (4)$$

Assignment of energy levels is based on the symmetry of the band profiles, *i.e.* $\Sigma-\Sigma$, $\Pi-\Pi$, etc. corresponding to a linear $D_{\infty h}$ molecule, and the rotational constant. For previously unreported states, the expected vibrational dependent rotational constant is given by the expression

$$B_v = B_e - \sum_i \alpha_i \left[v_i + \frac{d_i}{2} \right] \quad (5)$$

where B_e is the equilibrium rotational constant, v_i represents the vibrational quantum number, α_i is the vibration–rotation parameter, and d_i is the degree of the degeneracy of the ith vibrational mode. In our analysis, the variant of Eq. (5) that is used is given by

$$B_v = B_0 - \sum_i \alpha_i * v_i \quad (6)$$

For known states the rotational constants and vibration–rotation parameters are taken from previous studies [25–28], while for new or unknown states the rotational constants are determined, to first order approximation, from vibration–rotation parameters

Table 8
Observed line positions in cm^{-1} assigned to the $5_0^1 13_1^1$ band of triacetylene.

Transition	Obs.	$o-c \times 10^4$	Transition	Obs.	$o-c \times 10^4$	Transition	Obs.	$o-c \times 10^4$
Pe(31)	3325.4377	27	Pe(7)	3327.5932	7	Re(17)	3329.7949	−12
Pf(31)	3325.4377	−6	Pf(7)	3327.5932	2	Rf(17)	3329.7949	−2
Pe(30)	3325.5281	22	Pe(6)	3327.6821	7	Re(18)	3329.8817	−16
Pf(30)	3325.5281	−10	Pf(6)	3327.6821	2	Rf(18)	3329.8817	−6
Pe(29)	3325.6181	14	Pe(5)	3327.7708	5	Re(19)	3329.9683	−22
Pf(29)	3325.6181	−17	Pf(5)	3327.7708	1	Rf(19)	3329.9683	−11
Pe(28)	3325.7098	23	Pe(4)	3327.8594	3	Re(20)	3330.0555	−20
Pf(28)	3325.7098	−6	Pf(4)	3327.8594	0	Rf(20)	3330.0555	−9
Pe(27)	3325.8004	23	Pe(3)	3327.9475	−3	Re(21)	3330.1426	−19
Pf(27)	3325.8004	−5	Pf(3)	3327.9475	−6	Rf(21)	3330.1426	−7
Pe(26)	3325.8924	38	Qe(1)	3328.2136	0	Re(22)	3330.2293	−20
Pf(26)	3325.8924	11	Qe(3)	3328.2136	7	Rf(22)	3330.2293	−8
Pe(25)	3325.9815	25	Qf(1)	3328.2136	−1	Re(23)	3330.3161	−20
Pf(25)	3325.9815	0	Qf(2)	3328.2136	−1	Rf(23)	3330.3161	−7
Pe(24)	3326.0729	36	Re(1)	3328.3909	2	Re(24)	3330.4020	−28
Pf(24)	3326.0729	12	Rf(1)	3328.3909	4	Rf(24)	3330.4020	−16
Pe(23)	3326.1626	31	Re(2)	3328.4795	5	Re(25)	3330.4895	−18
Pf(23)	3326.1626	8	Rf(2)	3328.4795	7	Rf(25)	3330.4895	−6
Pe(22)	3326.2521	24	Re(3)	3328.5670	−3	Re(26)	3330.5766*	−12
Pf(22)	3326.2521	3	Rf(3)	3328.5670	0	Rf(26)	3330.5766*	1
Pe(21)	3326.3418	21	Re(4)	3328.6548	−7	Re(27)	3330.6624*	−19
Pf(21)	3326.3418	0	Rf(4)	3328.6548	−4	Rf(27)	3330.6624*	−6
Pe(20)	3326.4326	29	Re(5)	3328.7428	−9	Re(28)	3330.7483	−22
Pf(20)	3326.4326	10	Rf(5)	3328.7428	−5	Rf(28)	3330.7483	−9
Pe(19)	3326.5221	24	Re(6)	3328.8306	−12	Re(29)	3330.8351	−16
Pf(19)	3326.5221	6	Rf(6)	3328.8306	−7	Rf(29)	3330.8351	−3
Pe(18)	3326.6121	27	Re(7)	3328.9183	−15	Re(30)	3330.9214	−14
Pf(18)	3326.6121	10	Rf(7)	3328.9183	−10	Rf(30)	3330.9214	−1
Pe(17)	3326.7017	25	Re(8)	3329.0056	−21	Re(31)	3331.0086*	−1
Pf(17)	3326.7017	9	Rf(8)	3329.0056	−15	Rf(31)	3331.0086*	12
Pe(16)	3326.7908	19	Re(9)	3329.0924*	−32	Re(32)	3331.0925	−21
Pf(16)	3326.7908	5	Rf(9)	3329.0924*	−26	Rf(32)	3331.0925	−8
Pe(15)	3326.8800	16	Re(10)	3329.1804*	−30	Re(33)	3331.1794	−9
Pf(15)	3326.8800	3	Rf(10)	3329.1804*	−23	Rf(33)	3331.1794	5
Pe(14)	3326.9694	15	Re(11)	3329.2694*	−18	Re(34)	3331.2644	−15
Pf(14)	3326.9694	2	Rf(11)	3329.2694*	−11	Rf(34)	3331.2644	−1
Pe(12)	3327.1483*	16	Re(12)	3329.3574	−15	Re(35)	3331.3510*	−4
Pf(12)	3327.1483*	6	Rf(12)	3329.3574	−7	Rf(35)	3331.3510*	10
Pe(11)	3327.2372	12	Re(13)	3329.4455	−10	Re(36)	3331.4358	−9
Pf(11)	3327.2372	3	Rf(13)	3329.4455	−2	Rf(36)	3331.4358	5
Pe(10)	3327.3260	8	Re(14)	3329.5327	−13	Re(37)	3331.5223	3
Pf(10)	3327.3260	−1	Rf(14)	3329.5327	−4	Rf(37)	3331.5223	17
Pe(9)	3327.4150	7	Re(15)	3329.6205	−10	Re(39)	3331.6918	−2
Pf(9)	3327.4150	−1	Rf(15)	3329.6205	0	Rf(39)	3331.6918	11
Pe(8)	3327.5038	4	Re(16)	3329.7073	−15			
Pf(8)	3327.5038	−3	Rf(16)	3329.7073	−5			

Lines which are blended and given less statistical weight in the fit are indicated by *.

estimated based on the known values of the analogous molecule, cyanodiacetylene (HC_5N) [35]. Spectral analysis of new bands is performed by fitting the observed transitions using least-squares analysis to determine tentative lower and upper state rotational constants, as well as the band origin. Based on the preliminary values, the state symmetry, and rotational constants estimated from Eq. (6), vibrational assignments are made for both the upper and lower states.

In addition to the known ν_5 fundamental mode of triacetylene, three hot bands built on the ν_5 mode due to known doubly degenerate bending vibrational modes (ν_{10}, ν_{11}, and ν_{13}) are assigned in the 3330 cm^{-1} region, and one hot band involving the ν_1 mode ($1_0^1 8_0^1 11_1^0$) is assigned in the 3314 cm^{-1} region. All four of the newly assigned bands show relatively weak Q-branches, and no observable intensity alternation, indicating that they are parallel transitions of Π–Π state symmetries. The assignment and rotational constants for the lower and upper states of each of the bands are summarized in Tables 2 and 3, and the observed transitions, their rotational assignments, and deviations for each band are given in Tables 4–11. From the rotational profiles, the rotational temperature of triacetylene is determined to be about 23 K. While from the observed excited modes, the vibrational temperature is estimated to be significantly higher at about 105 K. This difference in temperatures was also noted by both Zhao et al. [22] and Chang and Nesbitt [23] for diacetylene, but it is to a much more substantial degree. Systematic rotational analyses on observed bands is then carried out in combination with previous infrared data [25,27,28].

3.1. The 5_0^1 fundamental

The strongest transitions in the experimental spectrum that are associated with triacetylene belong to the known perturbed ν_5 C—H asymmetric stretch mode, with a band origin at ~3329.05 cm^{-1} [26], and include newly observed transitions to a perturbing state, which have a band origin at ~3328.85 cm^{-1}. The 5_0^1 band is a parallel band of symmetry type $\Sigma_u^+ - \Sigma_g^+$, and exhibits the characteristic intensity alternation due to the 3:1 ortho (J = even) and para (J = odd) nuclear spin statistical weights for equivalent H atoms. However, from J' = 20 to 24, the intensity deviates from that expected due to intensity borrowing by the perturber state. The room temperature spectrum of the ν_5 fundamental has been studied extensively by Matsumura et al.

Table 9
Observed line positions in cm^{-1} assigned to the $5_0^1 10_1^1$ band of triacetylene.

Transition	Obs.	$o-c \times 10^4$	Transition	Obs.	$o-c \times 10^4$	Transition	Obs.	$o-c \times 10^4$
Pe(29)	3325.9877	11	Pe(9)	3327.7843*	5	Re(13)	3329.8151	−2
Pf(29)	3325.9877	0	Pf(9)	3327.7843*	2	Rf(13)	3329.8151	2
Pe(28)	3326.0774	0	Pe(8)	3327.8733	3	Re(14)	3329.9033	5
Pf(28)	3326.0774	−10	Pf(8)	3327.8733	1	Rf(14)	3329.9033	9
Pe(27)	3326.1694	14	Pe(7)	3327.9623	4	Re(15)	3329.9901	−1
Pf(27)	3326.1694	4	Pf(7)	3327.9623	2	Rf(15)	3329.9901	4
Pe(26)	3326.2587	1	Pe(6)	3328.0509	1	Re(16)	3330.0774	−2
Pf(26)	3326.2587	−9	Pf(6)	3328.0509	−1	Rf(16)	3330.0774	3
Pe(25)	3326.3501	11	Pe(5)	3328.1402	6	Re(17)	3330.1644	−4
Pf(25)	3326.3501	2	Pf(5)	3328.1402	4	Rf(17)	3330.1644	1
Pe(24)	3326.4398	6	Pe(4)	3328.2293	9	Re(18)	3330.2523	4
Pf(24)	3326.4398	−3	Pf(4)	3328.2293	7	Rf(18)	3330.2523	9
Pe(23)	3326.5302	7	Pe(3)	3328.3180	9	Re(19)	3330.3383	−7
Pf(23)	3326.5302	−1	Pf(3)	3328.3180	8	Rf(19)	3330.3383	−2
Pe(22)	3326.6189	−7	Pe(2)	3328.4057	−1	Re(20)	3330.4256*	−4
Pf(22)	3326.6189	−16	Pf(2)	3328.4057	−2	Rf(20)	3330.4256*	2
Pe(21)	3326.7104	7	Qe(1)	3328.5829	1	Re(21)	3330.5114*	−15
Pf(21)	3326.7104	−1	Qe(2)	3328.5829	3	Rf(21)	3330.5114*	−9
Pe(20)	3326.7992	−5	Qf(1)	3328.5829	1	Re(23)	3330.6848*	−16
Pf(20)	3326.7992	−12	Qf(3)	3328.5829	2	Rf(23)	3330.6848*	−9
Pe(19)	3326.8897	2	Re(2)	3328.8466	−15	Re(24)	3330.7732*	2
Pf(19)	3326.8897	−5	Rf(2)	3328.8466	−14	Rf(24)	3330.7732*	9
Pe(18)	3326.9785	−8	Re(3)	3328.9359	−4	Re(26)	3330.9462*	3
Pf(18)	3326.9785	−14	Rf(3)	3328.9359	−3	Rf(26)	3330.9462*	11
Pe(17)	3327.0696*	6	Re(4)	3329.0231	−14	Re(27)	3331.0317	−5
Pf(17)	3327.0696*	0	Rf(4)	3329.0231	−13	Rf(27)	3331.0317	3
Pe(16)	3327.1584	−2	Re(5)	3329.1108*	−19	Re(28)	3331.1183	−1
Pf(16)	3327.1584	−7	Rf(5)	3329.1108*	−17	Rf(28)	3331.1183	7
Pe(15)	3327.2482	0	Re(7)	3329.2883	−5	Re(30)	3331.2898	−5
Pf(15)	3327.2482	−5	Rf(7)	3329.2883	−3	Rf(30)	3331.2898	3
Pe(14)	3327.3378	2	Re(8)	3329.3773	6	Re(31)	3331.3749	−12
Pf(14)	3327.3378	−3	Rf(8)	3329.3773	9	Rf(31)	3331.3749	−3
Pe(13)	3327.4273	3	Re(9)	3329.4653	7	Re(32)	3331.4617	−1
Pf(13)	3327.4273	−2	Rf(9)	3329.4653	10	Rf(32)	3331.4617	8
Pe(12)	3327.5164	1	Re(10)	3329.5529	6	Re(33)	3331.5479	6
Pf(12)	3327.5164	−3	Rf(10)	3329.5529	9	Rf(33)	3331.5479	15
Pe(11)	3327.6062	6	Re(11)	3329.6402	2	Re(34)	3331.6313	−14
Pf(11)	3327.6062	2	Rf(11)	3329.6402	5	Rf(34)	3331.6313	−5
Pe(10)	3327.6941*	−6	Re(12)	3329.7279	2			
Pf(10)	3327.6941*	−10	Rf(12)	3329.7279	6			

Lines which are blended and given less statistical weight in the fit are indicated by *.

Table 10
Observed line positions in cm^{-1} assigned to the $5_0^1 11_1^1$ band of triacetylene.

Transition	Obs.	$o-c \times 10^4$	Transition	Obs.	$o-c \times 10^4$
Pe(17)	3327.4874*	2	Re(9)	3329.8807*	16
Pf(17)	3327.4874*	−2	Rf(9)	3329.8807*	17
Pe(16)	3327.5772*	4	Re(10)	3329.9663*	−4
Pf(16)	3327.5772*	1	Rf(10)	3329.9663*	−3
Pe(13)	3327.8455	6	Re(11)	3330.0557*	15
Pf(13)	3327.8455	4	Rf(11)	3330.0557*	16
Pe(12)	3327.9321*	−20	Re(12)	3330.1408	−8
Pf(12)	3327.9321*	−22	Rf(12)	3330.1408	−7
Pe(11)	3328.0211*	−22	Re(13)	3330.2276*	−13
Pf(11)	3328.0211*	−24	Rf(13)	3330.2276*	−12
Pe(10)	3328.1128*	5	Re(17)	3330.5754*	−24
Pf(10)	3328.1128*	3	Rf(17)	3330.5754*	−22
Pe(8)	3328.2893*	−11	Re(19)	3330.7508*	−8
Pf(8)	3328.2893*	−12	Rf(19)	3330.7508*	−7
Pe(7)	3328.3797*	5	Re(21)	3330.9243*	−11
Pf(7)	3328.3797*	3	Rf(21)	3330.9243*	−10
Pe(6)	3328.4668	−12	Re(25)	3331.2736*	17
Pf(6)	3328.4668	−13	Rf(25)	3331.2736*	17
Re(3)	3329.3535	14	Re(26)	3331.3585	1
Rf(3)	3329.3535	14	Rf(26)	3331.3585	2
Re(4)	3329.4416	14	Re(27)	3331.4432	−16
Rf(4)	3329.4416	15	Rf(27)	3331.4432	−16
Re(5)	3329.5291	11	Re(28)	3331.5322	10
Rf(5)	3329.5291	11	Rf(28)	3331.5322	11
Re(7)	3329.7026*	−12			
Rf(7)	3329.7026*	−11			

Lines which are blended and given less statistical weight in the fit are indicated by *.

[26], and is noted to have two strong perturbations, at $J' = 20$, and at $J' = 50$ and 54, as well as two weaker perturbations at $J' < 10$ and $J' > 110$. To date the identity or even the state symmetry of the perturbing levels has remained unclear. Here a perturbation analysis of the 5_0^1 band is performed using the combination of low-J ($J' \leqslant 39$) transitions observed in our jet-cooled spectrum with high-J ($39 < J' \leqslant 130$) transitions by Matsumura et al. [26].

The ground state rotational constant is determined by lower state combination differences to be $B_0 = 0.0441735(12)\,cm^{-1}$, which is in agreement with the values determined by Matsumura et al. [29] from the 11_0^1 band, and by McNaughton and Bruge [25] from the cold bands 5_0^1, 6_0^1, 11_0^1, $8_0^1 11_0^1$. It is also within three times the standard deviation of the values determined by Matsumura et al. [26] from 5_0^1 without taking into account perturbations and by Haas et al. [27] from analysis of the ν_{13} $v = 1$, 2, and 3 modes.

The upper state rotational constants for the ν_5 $v = 1$ state are determined by starting from the previously determined rotational constants by Matsumura et al. [26], and including either a heterogeneous or homogeneous perturbation coupling constant in the Hamiltonian. It is noted that given the weak perturbation at $J' < 10$, those transitions are given half the statistical weight of the other transitions in the fit. By varying the infrared intensity of the transitions to the perturbing state in PGOPHER [34], the simulated intensities of the transitions to the ν_5 state could reasonably

reproduce the observed experimental data. For both types of perturbation, the perturbing state was determined to not belong to a dark state, and has an infrared intensity of about 0.1 compared to the ν_5 state's infrared intensity of 1. As a result of the perturbation analysis of ν_5, extra lines which are due to transitions between the ground state and the perturbing level are identified for the first time (Tables 6 and 7).

Simultaneous least-squares fitting of the transitions to the ν_5 states, the transitions to the perturbing state, and the coupling coefficient results in the best fit parameters, which are given in Table 2. The determined ν_5 $v=1$ state rotational constants are consistent for the two types of perturbation fits, and gives a rotation–vibration parameter $\alpha_5 \sim 3.58(6)\times10^{-5}$. Furthermore, in both perturbation analyses of the 5_0^1 band the higher order rotational terms H and L have to be included to give the best fit, particularly for high-J transitions; this suggests that the molecule is quite stretchable. From the unweighted observed–calculated (o–c) values without considering the interaction between the two upper levels, *i.e.* the coupling constant set to zero (upper panels of Fig. 2), we confirm that the new transitions belong to the same progression, and both bands shows clear evidence of corresponding "avoided crossing" at $J'=21$ due to coupling to a perturbing rotational progression. Additionally, identical shifts in both the P- and R-branches in transitions with access to the same upper state, for both bands, unambiguously identify that the interaction takes place in the vibrationally excited state.

As noted earlier, the type of interaction between the ν_5 state and the perturbing state can be either a heterogeneous, *i.e.* a Coriolis interaction, or homogeneous perturbation, *i.e.* a Fermi resonance, which would present spectroscopically differently. The largest perturbation seen in both the jet-cooled spectrum and the room-temperature spectrum of Matsumura et al. [26] is rotationally "local" around $J'=21$, which suggests a Coriolis interaction, a type of L uncoupling perturbation, between the ν_5 state (Σ_u^+) and a Π_u vibrational state. The band origin and rotational constant for the ν_5 $v=1$ state are determined from least-squares analysis to be $\nu=3329.0544(1)\,\mathrm{cm}^{-1}$, and $B'=0.0441377(2)\,\mathrm{cm}^{-1}$, while the parameters of the perturbing level are determined to be $\nu=3328.8584(2)\,\mathrm{cm}^{-1}$ and $B'=0.0443102(14)\,\mathrm{cm}^{-1}$. The Coriolis coupling coefficient is determined to be $\zeta=6.86(5)\times10^{-4}\,\mathrm{cm}^{-1}$, which based on the resulting fit (left lower panel of Fig. 3), and the residuals after the fit (lower left panel of Fig. 2) well reproduces the intensities and positions of transitions in both bands. The defining feature of the Coriolis interaction is that the transition to the perturbing level is a perpendicular transition (Π–Σ) with a Q-branch. Unfortunately, as seen in the upper left panel of Fig. 3, the Q-branch is too weak to be discerned in the experimental spectrum.

An alternative cause of the perturbation is that it is the result of a Fermi resonance between the ν_5 state and a Σ_u^+ vibrational state that are very close in energy, and the rotational constants of the two levels are significantly different. In this case, the transition to the perturbing level is a parallel transition (Σ–Σ), which has no Q-branch, as seen in the upper right panel in Fig. 3. A Fermi resonance though, unlike the Coriolis interaction, effects the whole band to varying degrees, and could thus account for the small residual shifts seen for $J'<10$ and leading up to $J'=21$. From least-squares analysis the ν_5 $v=1$ state band origin and rotational constant are determined to be $\nu=3329.0521(1)\,\mathrm{cm}^{-1}$ and $B'=0.0441377(2)\,\mathrm{cm}^{-1}$, respectively. The corresponding perturbing state band origin and rotational constants are determined from the fit to be $\nu=3328.8435(2)\,\mathrm{cm}^{-1}$ and $B'=0.0445931(32)\,\mathrm{cm}^{-1}$, both of which fit the requirements for a Fermi resonance with level crossing. The Fermi coupling coefficient is determined to be $W=0.0218(2)\,\mathrm{cm}^{-1}$, and from the resulting fit (the right panels of Fig. 3), and the residuals after the fit (the lower right panel of Fig. 2) it is shown that a Fermi resonance offers as good a fit as the Coriolis interaction.

Table 11
Observed line positions in cm^{-1} assigned to the $1_0^1 8_0^1 11_1^0$ band of triacetylene.

Transition	Obs.	$o-c\times10^4$	Transition	Obs.	$o-c\times10^4$
Pe(22)	3308.8532	4	Re(4)	3311.2511	−3
Pf(22)	3308.8532	3	Rf(4)	3311.2511	−2
Pe(21)	3308.9427	4	Re(5)	3311.3376	−18
Pf(21)	3308.9427	3	Rf(5)	3311.3376	−17
Pe(20)	3309.0327	8	Re(6)	3311.4265	−9
Pf(20)	3309.0327	7	Rf(6)	3311.4265	−7
Pe(19)	3309.1199	−14	Re(7)	3311.5146	−7
Pf(19)	3309.1199	−16	Rf(7)	3311.5146	−5
Pe(18)	3309.2109	2	Re(8)	3311.6023	−8
Pf(18)	3309.2109	0	Rf(8)	3311.6023	−6
Pe(17)	3309.3007	6	Re(9)	3311.6903	−6
Pf(17)	3309.3007	5	Rf(9)	3311.6903	−4
Pe(16)	3309.3898	4	Re(10)	3311.7781	−5
Pf(16)	3309.3898	2	Rf(10)	3311.7781	−2
Pe(14)	3309.5694	16	Re(11)	3311.8660	−2
Pf(14)	3309.5694	14	Rf(11)	3311.8660	0
Pe(12)	3309.7469	8	Re(12)	3311.9532	−7
Pf(12)	3309.7469	7	Rf(12)	3311.9532	−4
Pe(11)	3309.8361	10	Re(13)	3312.0410	−4
Pf(11)	3309.8361	9	Rf(13)	3312.0410	−1
Pe(10)	3309.9231*	−9	Re(14)	3312.1277	−12
Pf(10)	3309.9231*	−10	Rf(14)	3312.1277	−9
Pe(9)	3310.0136	7	Re(15)	3312.2152	−12
Pf(9)	3310.0136	6	Rf(15)	3312.2152	−8
Pe(8)	3310.1024	6	Re(16)	3312.3037	−1
Pf(8)	3310.1024	5	Rf(16)	3312.3037	3
Pe(7)	3310.1911	5	Re(17)	3312.3914	3
Pf(7)	3310.1911	4	Rf(17)	3312.3914	8
Pe(6)	3310.2802	9	Re(18)	3312.4774	−10
Pf(6)	3310.2802	8	Rf(18)	3312.4774	−5
Pe(5)	3310.3688	9	Re(19)	3312.5649	−6
Pf(5)	3310.3688	8	Rf(19)	3312.5649	−1
Re(3)	3311.1634	1	Re(20)	3312.6518	−9
Rf(3)	3311.1634	2	Rf(20)	3312.6518	−4

Lines which are blended and given less statistical weight in the fit are indicated by *.

The residuals for the two fits are of the same order of magnitude, which means that the perturbing state is as likely to be Σ or Π symmetry. The uncertainty in the line positions is on average $<0.0015\,\mathrm{cm}^{-1}$, but ranges from about -0.005 to $0.005\,\mathrm{cm}^{-1}$, which is greater than the experimental uncertainty. This error is likely a result of two additional weak perturbing states at $J'=1$ and $J'=27$ that are not included in the fits. The positive fractional change in $\Delta B/B$ (~+0.3% and 1% for the Coriolis interaction and Fermi resonance fits, respectively) with respect to the unperturbed excited state seen for either perturbation fit suggests that the perturbed state decreases the moment of inertia for end-over-end rotation, which is consistent with a vibrational bending of the CCCCCC backbone. Recently, Chang and Nesbitt [23] found a similar type of perturbing state for diacetylene, which, while much weaker than the one seen for triacetylene, is determined to be a Coriolis interaction. As with diacetylene, the large density of states of triacetylene around $3330\,\mathrm{cm}^{-1}$, and the number of unknown vibration–rotation constants hinders definitive assignment of the perturbing state [23,26]. However, since the state density and excited hot bands are dominated by the lowest frequency modes, it is likely that the perturbing state is a combination vibrational level involving the excitation of ν_{10} and/or ν_{13}.

3.2. The $5_0^1 10_1^1$ and $5_0^1 13_1^1$ bands

A series of three hot bands built on the ν_5 C—H asymmetric stretch fundamental is observed in the $3330\,\mathrm{cm}^{-1}$ region, all due

to doubly degenerate bending vibrations (Table 3). The most intense of the series is assigned to the $5_0^1 13_1^1$ hot band, which is about 50% the intensity of the 5_0^1 band, and has an observed Q-branch at 3328.2137(2) cm^{-1}. The upper state rotational constant is determined from least-squares analysis to be B' = 0.0442268(7) cm^{-1}, which from Eq. 6 is in agreement with a the combination state of $5^1 13^1$. The lower state is consequently v_{13} v = 1 (Π_u), and has been accurately determined by Haas et al. [27]; we fix the lower state parameters to values derived there in order to give the best fit to the line positions.

Given the similar rotational constants and vibration–rotation parameters between the v_{10} C≡C—C symmetric bending mode and the v_{13} C≡C—C asymmetric bending modes, it is challenging to distinguish between these two options. Fortunately, the presence of a second hot band centered at 3328.5829(2) cm^{-1} with a determined upper state B' = 0.0442216(9) cm^{-1}, which is consistent with the value estimated for $5^1 10^1$ from Eq. (6), clarifies the assignment of the two bands. Additionally, from least-squares fitting the v_{10} v = 1 (Π_g) lower state is found to have a rotational constant B'' = 0.0442534(7) cm^{-1}, which is in agreement with the values found by McNaughton and Bruget [25], who observed the mode as part of the $11_0^1 10_1^1$ and $8_0^1 11_0^1 10_1^1$ hot bands. The $5_0^1 10_1^1$ band is a factor 2.5 weaker compared to the $5_0^1 13_1^1$ band, with a relative intensity of about 15% that of the 5_0^1 band. It is noted that for both the $5_0^1 10_1^1$ and the $5_0^1 13_1^1$ band the *o–c* deviations are of the order of or smaller than the experimental accuracy, but show a particular structure, *e.g.* the P-branch *o–c* values being predominantly positive while the R-branch *o–c* values are negative. This identical trend seen for both bands cannot be accounted for by including higher order terms, and is likely due to an error in the frequency calibration, which is associated with small temperature fluctuations during spectral recording.

3.3. The $5_0^1 11_1^1$ and $1_0^1 8_0^1 11_1^0$ bands

The $5_0^1 11_1^1$ and the $1_0^1 8_0^1 11_1^0$ bands share the v_{11} v = 1 (Π_u) ground state, which has been studied by Haas et al. [28], and we have fixed the lower state to values derived there. A series of nine transitions, and another sixteen transitions which are blended by other lines, is tentatively assigned to the $5_0^1 11_1^1$ band centered at 3328.9994(2) cm^{-1}. Additionally, the band is particularly weak with an intensity of about 8% relative to the 5_0^1 band. Given the limited number of observed transitions, the upper state rotational constant is determined by least-squares fit to be B' = 0.0441465(6) cm^{-1}, which from Eq. (6) is assigned to the $5^1 11^1$ state.

The $1_0^1 8_0^1 11_1^0$ (Π_u—Π_g) band, centered at 3310.8104(2) cm^{-1}, is the only band not associated with the C—H asymmetric stretch mode, and is instead a combination of the v_1 C—H symmetric stretch fundamental mode and two CCC bending modes. The band is the weakest observed band of triacetylene at about 5% the intensity of the v_5 fundamental band. As a result of the weak intensity of the band, the line positions are confirmed by comparison of the spectrum in this work and the spectrum recorded by our group which favored diacetylene [22], and noting consistent changes in line intensities. In this manner, thirty unblended transitions are identified for $1_0^1 8_0^1 11_1^0$. Least-squares analysis determined an upper state rotational constant B' = 0.0441528(9) cm^{-1}, which is consistent with the B_v value determined for the $1^1 8^1$ state from Eq. (6).

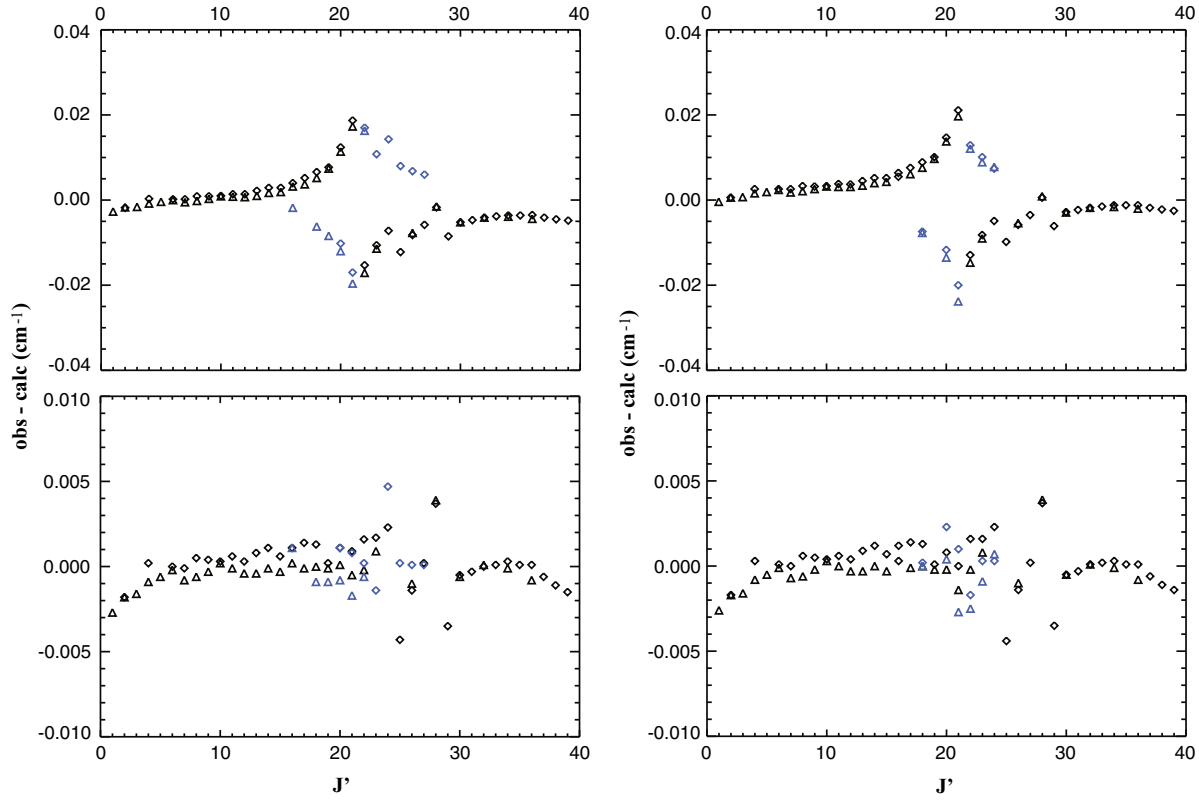

Fig. 2. Observed perturbation in the v_5 state at about J'' = 20. The unweighted observed–calculated (*o–c*) values of the v_5 fundamental transitions are plotted in black, and the perturber state transitions are plotted in blue. Additionally, R-branch transitions are plotted with diamonds and P-branch transitions are plotted with triangles. The top panels show the *o–c* deviations of the transitions without Coriolis interaction taken into account (left), and of the transitions without Fermi resonance taken into account (right). The bottom panels show the *o–c* deviations of the transitions with Coriolis interaction taken into account (left) and of the transitions with Fermi resonance taken into account (right). Note the different scales between the top and bottom panels. (For interpretation of the references to colour in this figure legend, the reader is referred to the web version of this article.)

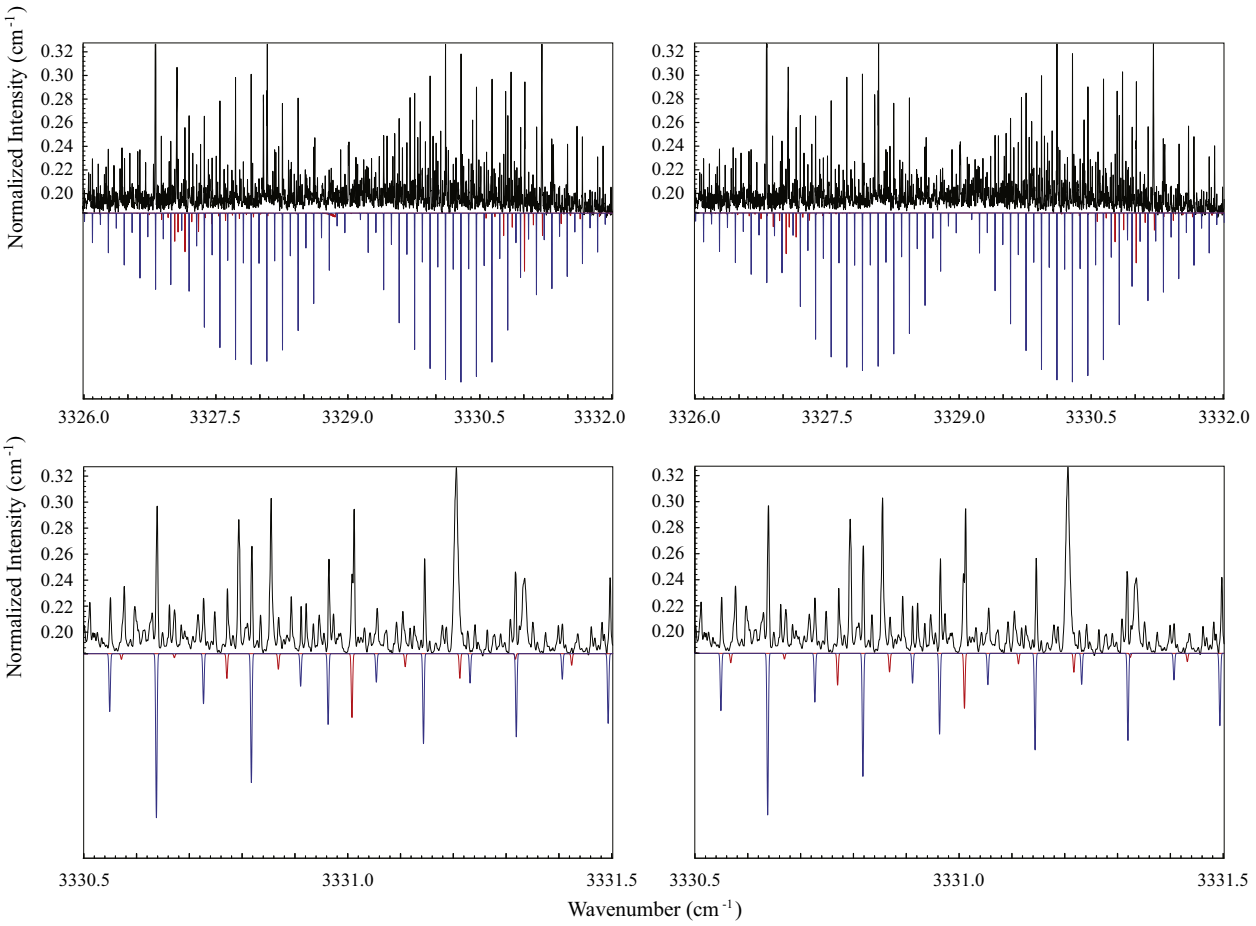

Fig. 3. Experimental spectrum shown in black with the simulated transitions to the v_5 state shown in blue, and the simulated transitions to the perturbing state shown in red. The top panels show the overall fit for the Coriolis interaction (left) and Fermi resonance (right), and bottom panels show a zoom in of the R-branch from R(16)–R(27) of the 5_0^1 band and from R(17)–R(25) of the perturber band. It is noted some of the assigned transitions are blended with transitions of other bands, such as those of HC_4H, which accounts for the discrepancies in intensity and line width, *e.g.* R(19) and R(20) of the perturbing band. (For interpretation of the references to colour in this figure legend, the reader is referred to the web version of this article.)

4. Conclusion

The current high-resolution study of triacetylene using cw-CRDS has yielded accurate measurements of the rotational constants for v_5 $v = 1$ state, taking into account the prominent perturbation, as well as the rotational constants of the perturbing state. While the perturber state of the 5_0^1 band still remain inconclusively identified, it has for the first time been observed and rotational constants have been determined, which suggest it is most likely a combination level of the low lying bending modes.

Four newly identified hot bands are also presented, and their rotational constants are reported. It is also found that, even under experimental conditions which favor the production of triacetylene over diacetylene, the number of observed hot bands of triacetylene is significantly less than that observed for diacetylene [22,23]. Furthermore, while the vibrational temperature of the produced triacetylene molecules is much greater than their rotational temperature, the difference is not as extreme as that seen for diacetylene [22,23], which suggests that comparatively triacetylene is more efficient at vibrational cooling. The same trend in efficient cooling through intermode vibration–vibration transfer due to an increase in state density is also seen for the cyanopolyynes, with cyanodiacetylene having a relatively lower vibrational temperature compared to cyanoacetylene [36].

While the modes seen here are less likely to be observed in astronomical objects compared to the lower excitation bending mode fundamentals, due to either low temperature of the environments or overlap with modes from other polyynes, accurate knowledge of their rotational spectra confirms earlier determinations of the rotational constants. This is of particular importance in the case of v_{10}, which has only been observed through hot or combination bands. Additionally, we have also more conclusively determined the ground state rotational constant for triacetylene, which can be in turn used to accurately predict the corresponding rotational constants of vibrational levels that, while not observed in the laboratory, could still be present in space, such as the v_{12} fundamental.

Acknowledgments

This work is financially supported by the Netherlands Organization for Scientific Research (NWO) through a VICI grant, the Netherlands Research School for Astronomy (NOVA), and has been performed within the context of the Dutch Astrochemistry Network.

References

[1] Y.L. Yung, M. Allen, J.P. Pinto, Astrophys. J. Suppl. 55 (1984) 465–506, http://dx.doi.org/10.1086/190963.
[2] K.-H. Homann, Angew. Chem. Int. Ed. 37 (18) (1998) 2434–2451, http://dx.doi.org/10.1002/(SICI)1521-3773(19981002)37:18<2434::AID-ANIE2434>3.0.CO;2-L. ISSN 1521-3773.

[3] J. Cernicharo, A.M. Heras, A.G.G.M. Tielens, J.R. Pardo, F. Herpin, M. Guélin, L.B.F.M. Waters, Astrophys. J. Lett. 546 (2001) L123–L126, http://dx.doi.org/10.1086/318871.
[4] V. Vuitton, C. Gée, F. Raulin, Y. Bénilan, C. Crépin, M.-C. Gazeau, Planet. Space Sci. 51 (2003) 847–852, http://dx.doi.org/10.1016/j.pss.2003.07.001.
[5] E. Wilson, S. Atreya, Planet. Space Sci. 51 (1415) (2003) 1017–1033, http://dx.doi.org/10.1016/j.pss.2003.06.003. surfaces and Atmospheres of the Outer Planets their Satellites and Ring Systems, ISSN 0032-0633. <http://www.sciencedirect.com/science/article/pii/S0032063303001338>.
[6] J. Bernard-Salas, E. Peeters, G.C. Sloan, J. Cami, S. Guiles, J.R. Houck, Astrophys. J. Lett. 652 (2006) L29–L32, http://dx.doi.org/10.1086/509777.
[7] V. Vuitton, J.-F. Doussin, Y. Bénilan, F. Raulin, M.-C. Gazeau, Icarus 185 (2006) 287–300, http://dx.doi.org/10.1016/j.icarus.2006.06.002.
[8] N. Sakai, S. Yamamoto, Chem. Rev. 113 (2013) 8981–9015, http://dx.doi.org/10.1021/cr4001308.
[9] M. Frenklach, D.W. Clary, W.C. Gardiner, S.E. Stein, in: Twentieth Symposium (International) on Combustion, vol. 887, The Combustion Institute, Pittsburgh, 1985.
[10] R.E. Bandy, C. Lakshminarayan, R.K. Frost, T.S. Zwier, Science 258 (1992) 1630–1633, http://dx.doi.org/10.1126/science.258.5088.1630.
[11] I. Cherchneff, J.R. Barker, A.G.G.M. Tielens, Astrophys. J. 401 (1992) 269–287, http://dx.doi.org/10.1086/172059.
[12] A. Krestinin, Combust. Flame 121 (3) (2000) 513–524, http://dx.doi.org/10.1016/S0010-2180(99)00167-4. ISSN 0010-2180. <http://www.sciencedirect.com/science/article/pii/S0010218099001674>.
[13] F. Stahl, P. Schleyer, H.F. Schaefer III, R. Kaiser, Planet. Space Sci. 50 (78) (2002) 685–692, http://dx.doi.org/10.1016/S0032-0633. exobiology: the search for extraterrestrial life and prebiotic ch emistry, ISSN 0032-0633. <http://www.sciencedirect.com/science/article/pii/S0032063302000144>.
[14] X. Gu, Y.S. Kim, R.I. Kaiser, A.M. Mebel, M.C. Liang, Y.L. Yung, Proc. Natl. Acad. Sci. 106 (38) (2009) 16078–16083, http://dx.doi.org/10.1073/pnas.0900525106. <http://www.pnas.org/content/106/38/16078.abstract>.
[15] V.G. Kunde, A.C. Aikin, R.A. Hanel, D.E. Jennings, W.C. Maguire, R.E. Samuelson, Nature 292 (1981) 686–688, http://dx.doi.org/10.1038/292686a0.
[16] L.M. Ziurys, Proc. Natl. Acad. Sci. 103 (33) (2006) 12274–12279, http://dx.doi.org/10.1073/pnas.0602277103. <http://www.pnas.org/content/103/33/12274.abstract>.
[17] M.C. McCarthy, C.A. Gottlieb, H. Gupta, P. Thaddeus, Astrophys. J. Lett. 652 (2006) L141–L144, http://dx.doi.org/10.1086/510238.
[18] K.W. Sattelmeyer, J.F. Stanton, J. Am. Chem. Soc. 122 (34) (2000) 8220–8227, http://dx.doi.org/10.1021/ja9940874.
[19] W.D. Langer, T. Velusamy, T.B.H. Kuiper, R. Peng, M.C. McCarthy, M.J. Travers, A. Kovács, C.A. Gottlieb, P. Thaddeus, Astrophys. J. Lett. 480 (1997) L63–L66, http://dx.doi.org/10.1086/310622.
[20] H. Suzuki, M. Ohishi, N. Kaifu, S.-I. Ishikawa, T. Kasuga, Astron. Soc. Jpn. Publ. 38 (1986) 911–917.
[21] S. Saito, K. Kawaguchi, H. Suzuki, M. Ohishi, N. Kaifu, S.-I. Ishikawa, Astron. Soc. Jpn. Publ. 39 (1987) 193–199.
[22] D. Zhao, K.D. Doney, H. Linnartz, J. Mol. Spectrosc. 296 (0) (2014) 1–8, http://dx.doi.org/10.1016/j.jms.2013.11.008. ISSN 0022-2852. <http://www.sciencedirect.com/science/article/pii/S0022285213001732>.
[23] C.-H. Chang, D.J. Nesbitt, J. Phys. Chem. A 0(0) (0) null, http://dx.doi.org/10.1021/acs.jpca.5b02310.
[24] E. Bjarnov, D. Christensen, O. Nielsen, E. Augdahl, E. Kloster-Jensen, A. Rogstad, Spectrochim. Acta Part A: Mol. Spectrosc. 30 (6) (1974) 1255–1262, http://dx.doi.org/10.1016/0584-8539(74)80110-8. ISSN 0584-8539. <http://www.sciencedirect.com/science/article/pii/0584853974801108>.
[25] D. McNaughton, D. Bruget, J. Mol. Spectrosc. 150 (2) (1991) 620–634, http://dx.doi.org/10.1016/0022-2852(91)90253-7. ISSN 0022-2852. <http://www.sciencedirect.com/science/article/pii/0022285291902537>.
[26] K. Matsumura, K. Kawaguchi, D. Mcnaughton, D. Bruget, J. Mol. Spectrosc. 158 (2) (1993) 489–493, http://dx.doi.org/10.1006/jmsp.1993.1095. ISSN 0022-2852. <http://www.sciencedirect.com/science/article/pii/S0022285283710957>.
[27] S. Haas, K. Yamada, G. Winnewisser, J. Mol. Spectrosc. 164 (2) (1994) 445–455, http://dx.doi.org/10.1006/jmsp.1994.1088. ISSN 0022-2852. <http://www.sciencedirect.com/science/article/pii/S0022285284710885>.
[28] S. Haas, G. Winnewisser, K. Yamada, K. Matsumura, K. Kawaguchi, J. Mol. Spectrosc. 167 (1) (1994) 176–190, http://dx.doi.org/10.1006/jmsp.1994.1224. ISSN 0022-2852. <http://www.sciencedirect.com/science/article/pii/S0022285284712240>.
[29] K. Matsumura, H. Kanamori, K. Kawaguchi, E. Hirota, T. Tanaka, J. Mol. Spectrosc. 131 (2) (1988) 278–287, http://dx.doi.org/10.1016/0022-2852(88)90239-1. ISSN 0022-2852. <http://www.sciencedirect.com/science/article/pii/0022285288902391>.
[30] D. Zhao, J. Guss, A.J. Walsh, H. Linnartz, Chem. Phys. Lett. 565 (0) (2013) 132–137, http://dx.doi.org/10.1016/j.cplett.2013.02.025. ISSN 0009-2614. <http://www.sciencedirect.com/science/article/pii/S0009261413002340>.
[31] T. Motylewski, H. Linnartz, Rev. Sci. Instrum. 70 (2) (1999) 1305–1312, http://dx.doi.org/10.1063/1.1149589. <http://scitation.aip.org/content/aip/journal/rsi/70/2/10.1063/1.1149589>.
[32] L. Rothman, I. Gordon, Y. Babikov, A. Barbe, D.C. Benner, P. Bernath, M. Birk, L. Bizzocchi, V. Boudon, L. Brown, A. Campargue, K. Chance, E. Cohen, L. Coudert, V. Devi, B. Drouin, A. Fayt, J.-M. Flaud, R. Gamache, J. Harrison, J.-M. Hartmann, C. Hill, J. Hodges, D. Jacquemart, A. Jolly, J. Lamouroux, R.L. Roy, G. Li, D. Long, O. Lyulin, C. Mackie, S. Massie, S. Mikhailenko, H. Mller, O. Naumenko, A. Nikitin, J. Orphal, V. Perevalov, A. Perrin, E. Polovtseva, C. Richard, M. Smith, E. Starikova, K. Sung, S. Tashkun, J. Tennyson, G. Toon, V. Tyuterev, G. Wagner, J. Quant. Spectrosc. Radiat. Transfer 130 (0) (2013) 4–50, http://dx.doi.org/10.1016/j.jqsrt.2013.07.002. {HITRAN2012} special issue, ISSN 0022-4073. <http://www.sciencedirect.com/science/article/pii/S0022407313002859>.
[33] G. Guelachvili, A. Craig, D. Ramsay, J. Mol. Spectrosc. 105 (1) (1984) 156–192, http://dx.doi.org/10.1016/0022-2852(84)90110-3. ISSN 0022-2852. <http://www.sciencedirect.com/science/article/pii/0022285284901103>.
[34] C.M. Western, PGOPHER Version 8.0, University of Bristol Research Data Repository, 2014. http://dx.doi.org/10.5523/bris.huflggvpcuc1zvliqed497r2. <http://pgopher.chm.bris.ac.uk/>.
[35] C. Degli Esposti, L. Bizzocchi, P. Botschwina, K.M.T. Yamada, G. Winnewisser, S. Thorwirth, P. Förster, J. Mol. Spectrosc. 230 (2005) 185–195, http://dx.doi.org/10.1016/j.jms.2004.11.010.
[36] M.E. Sanz, M.C. Mccarthy, P. Thaddeus, J. Chem. Phys. 122 (19) (2005) 194319, http://dx.doi.org/10.1063/1.1869988. ISSN 0021-9606.